THE JOURNAL OF PHYSICAL CHEMISTRY B

Article

pubs.acs.org/JPCB

Effect of Ionic Aqueous Environments on the Structure and Dynamics of the $A\beta_{21-30}$ Fragment: A Molecular-Dynamics Study

Micholas Dean Smith and Luis Cruz*

Department of Physics, 3141 Chestnut Street, Drexel University, Philadelphia, Pennsylvania 19104, United States

Supporting Information

ABSTRACT: The amyloid β-protein (Aβ) has been implicated in the pathogenesis of Alzheimer's disease. The role of the structure and dynamics of the central $A\beta_{21-30}$ decapeptide region of the full-length Aβ is considered crucial in the aggregation pathway of Aβ. Here we report results of isobaric−isothermal (NPT) all-atom explicit water molecular dynamics simulations of the monomeric form of the wild-type $A\beta_{21-30}$ fragment in aqueous salt environments formed by neurobiologically important group IA (NaCl, KCl) and group IIA ($CaCl_2$, $MgCl_2$) salts. Our simulations reveal the existence of salt-specific changes to secondary structure propensities, lifetimes, hydrogen bonding, salt-bridge formation, and decapeptide−ion contacts of this decapeptide. These results suggest that aqueous environments with the $CaCl_2$ salt, and to a much lesser extent the $MgCl_2$ salt, have profound effects by increasing random coil structure propensities and lifetimes and diminishing intrapeptide hydrogen bonding. These effects are rationalized in terms of direct cation−decapeptide contacts and changes to the hydration-shell water molecules. On the other side of the spectrum, environments with the NaCl and KCl salts have little influence on the decapeptide's secondary structure despite increasing hydrogen bonding, salt-bridge formation, and lifetime of turn structures. The observed enhancement of open structures by group IIA may be of importance in the folding and aggregation pathway of the full-length Aβ.

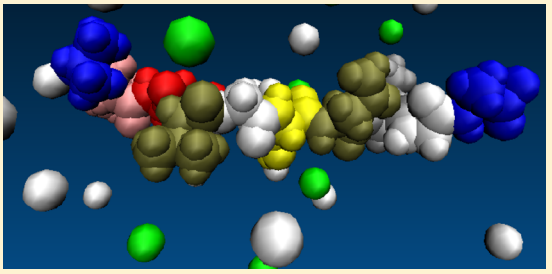

INTRODUCTION

Alzheimer's disease is a neurodegenerative disorder characterized by neuronal cell death, extracellular amyloid rich plaques, and intraneuronal neurofibrillary tangles. Work by Hardy[1,2] introduced the amyloid cascade hypothesis which posited that deposition of the 40/42 residue amyloid β-protein (Aβ) acted as a first step in the development of amyloid fibrils that triggered the development of characteristic senile plaques and subsequent cell death. Recent studies,[3−10] however, have since called for a revision to this hypothesis stating instead that prefibrillar oligomeric aggregates of Aβ are the dominant neurotoxic agents.

The implication of the prefibrillar oligomers as neurotoxic agents suggests a plausible direction for control of the disease: block the pathways by which monomeric Aβ peptides oligomerize. One way to achieve this goal is to determine the intrapeptide interactions that act to destabilize the monomeric form of Aβ and result in the formation of oligomers, and with this knowledge develop a strategy to prevent monomer destabilization. To this end, experimental[11] and computational studies[12,13] have addressed the folding and oligomerization of both $A\beta_{1-40}$ and $A\beta_{1-42}$ (for a current review of the field, see ref 14 and references therein). However, it has proven difficult to experimentally determine the precise structure of monomers and early stage oligomers for Aβ, as it belongs to a class of intrinsically disordered proteins[15,16] where partially ordered Aβ conformers are transient and unstable.[17,18] In addition, the high aggregation propensity of Aβ makes experimental work particularly difficult; though both *in silico* and *in vitro* studies of fragments and related peptides, along with their respective pathological mutations (all of which preserve properties of the full-length protein), have shown promise in overcoming some of these difficulties and provided important structural information regarding Aβ.[19−34]

Of the wide variety of Aβ monomer fragments studied, the $A\beta_{21-30}$ is of particular interest. This central decapeptide region of the full-length Aβ protein was determined by Lazo et al.[35] to be a protease resistant core in both $A\beta_{1-40}$ and $A\beta_{1-42}$, and was further characterized as protease resistant as an isolated decapeptide. This decapeptide has loop structures mostly stabilized by a combination of intrapeptide hydrogen bonds (HBs), hydrophobic packing between its forth and eighth residues, and intrapeptide electrostatic interactions (salt-bridges)[36−41] and also contains weakly populated β hairpin structures,[42,43] that taken together with the work by Lazo et al. suggest that the decapeptide may act as a nucleation site for the folding dynamics of the full-length peptide, as shown in other systems.[44] In addition, simulations[36,38,41−43] and experiments[40] have also shown the existence of metastable β secondary structures, salt-bridges between the Glu22/Asp23 and Lys28 residues, and HBs between Asp23−Ser26/Asn27, and have further shown that the $A\beta_{21-30}$ can be classified into three

Received: December 21, 2012
Revised: May 13, 2013
Published: May 15, 2013

   dx.doi.org/10.1021/jp312653h | J. Phys. Chem. B 2013, 117, 6614−6624

families of secondary structures: loop1/turn, loop2/β-(hairpin/bridge), and open/coil.[39]

A simplifying assumption used in previous computational works has been to model the *in vivo*/*in vitro* environmental conditions of the peptide as a pure water environment. This idealized environment, however, lacked important conditions present *in vivo*. The full-length Aβ peptide is produced in the extracellular space by the proteolytic cleavage of the membrane bound amyloid precursor protein (APP) at its 671st and near its 710th residues of the protein. This cleavage is performed by a combination of β- and γ-secretase, where the β-secretase cleaves a small extracellular peptide from the protein and remains bound to the membrane, and γ-secretase releases the peptide into the extracellular space producing Aβ.[45] Because the extracellular membrane environment has a variety of ion channels associated with transmembrane transport, it is reasonable to assume that this region has high local concentrations of dissociated group IA and IIA chloride salts. Moreover, recent *in vitro* studies of the Aβ peptide with group IA, IIA, and Zn^{2+} salts[46−50] have shown that at both prefibril and postfibril stages changes to the structure and kinetics of the oligomeric forms of the full-length peptide are found. These results and others of similar ionic nature serve as the motivation to study whether environments rich in salt modify the intrapeptide and solvent−peptide interactions that dominate the monomeric form of Aβ.

Here, using all-atom molecular dynamics (MD) simulations with explicit solvent, we explore the influence of biologically common group IA and IIA chloride salts on intrapeptide interactions and their possible influence on the structural dynamics of the Aβ_{21-30} monomer. Of particular interest is the exploration of changes in the decapeptide's structural dynamics and lifetimes of long-lived structural motifs found by Cruz et al.[42] when in environments rich with KCl, $MgCl_2$, $CaCl_2$, or NaCl at a variety of concentrations (0.1−0.5 M). Our results show that $CaCl_2$ environments have an enhancement effect on the prevalence of disordered structures, while both $MgCl_2$ and $CaCl_2$ environments increase the lifetimes of these structures. KCl environments, on the other hand, display a negligible effect on the lifetimes of the disordered structures and provide an increase to the lifetimes of turn structures accompanied by an increased number of intrapeptide HBs. NaCl environments are found to provide similar effects to KCl environments, though the strength of these effects is weaker. Possible mechanisms by which cation-specific interactions influence the structural dynamics of Aβ_{21-30} are examined.

METHODS

Simulations. The peptide used in this study is the 10 amino acid Aβ_{21-30} decapeptide with the primary structure Ala21-Glu22-Asp23-Val24-Gly25-Ser26-Asn27-Lys28-Gly29-Ala30 with charged termini and a net charge of −1. To study the dynamics of the Aβ_{21-30} decapeptide in aqueous salt environments, we used all-atom MD simulations with explicit solvent. These simulations were performed under isobaric−isothermal (NPT) conditions using the GROMACS 4.0.7[51−53] simulation package with the OPLS-AA force field[54,55] and the TIP3P water model.[56,57] Temperature and pressure coupling was maintained using the Berendsen thermo/barostats[58] with a simulation temperature of 283 K and a pressure of 1 atm. The specific temperature of 283 K was chosen to correspond to previous experimental[35] and computational work.[36,42] Salt environments were prepared by first placing the decapeptide in the center of a cubic periodic box with sides of approximately 43 Å, followed by solvation of the decapeptide using TIP3P water molecules. To obtain salt concentrations equivalent to 0.1, 0.2, 0.3, 0.4, and 0.5 M (and to obtain a net system charge of 0), individual TIP3P water molecules were removed and replaced with dissolved ionic species: $CaCl_2$, $MgCl_2$, KCl, or NaCl (see Table 1). All simulation trajectories were started using one of two initial Aβ_{21-30} conformations: a β-hairpin or a random coil. These two initial structures were chosen to allow for comparison to previously reported results on the structure and dynamics of the decapeptide[36,37,43] and the metastability and lifetimes of the β-hairpin (β_{28}) conformations recently reported by Cruz et al.[42]

Table 1. Number of Water Molecules That Were Replaced by Salt Ions to Obtain Specified Ionic Concentrations

concentration	salt	no. of waters replaced
0.1 M	$CaCl_2$/$MgCl_2$	14
	KCl/NaCl	9
0.2 M	$CaCl_2$/$MgCl_2$	29
	KCl/NaCl	19
0.3 M	$CaCl_2$/$MgCl_2$	44
	KCl/NaCl	29
0.4 M	$CaCl_2$/$MgCl_2$	59
	KCl/NaCl	39
0.5 M	$CaCl_2$/$MgCl_2$	74
	KCl/NaCl	49

Simulation trajectories were generated following a three-step process: a steepest decent energy minimization, relaxation with position restraints, and generation of production runs. The energy minimization step was achieved by performing 0.1 ps of steepest descent steps with a time step of 1 fs and a maximum of 1000 steps. Following energy minimization, short-time (20 ps) all-atom simulations with time steps of 2 fs with decapeptide position restraints (using SETTLE and LINCS)[59,60] were performed. Production runs were generated using a 4 fs time step (facilitated by GROMACS), while positions and energies of all simulated atoms were recorded at 4 ps intervals and a running time of 400 ns. To verify that the 4 fs time step trajectories gave equivalent results to the more standard 2 fs time step trajectories, five 200 ns trajectories under pure water conditions using 2 fs time steps were generated and compared to equivalent trajectories using a 4 fs time step. Comparison of distributions of secondary structure between these two time steps did not reveal significant differences (Figure S1, Supporting Information).

For the trajectories with β initial conditions, a β-hairpin of the form β_{28} found in Cruz et al.[42] (hairpin structures characterized by HBs between Glu22(O)−Lys28(H), Ser26-(O)−Val24(H), and Ala30(O)−Ala21(H)) was selected and followed the same simulation scheme as that of the random coil initial condition trajectories described above with one crucial exception: trajectories with β initial conditions were run until the peptide exited the β-hairpin structure. Exiting of the β-hairpin structure was characterized by a sudden increase in the root-mean squared deviation (RMSD) of the peptide's structure from its initial configuration (see Figure S2, Supporting Information), though this abrupt change in RMSD in general gave only an approximation to the exit time of the β-hairpin. To attain a better estimate, lifetimes of

dx.doi.org/10.1021/jp312653h | J. Phys. Chem. B 2013, 117, 6614−6624

Table 2. Simulation Time per Trajectory[a]

concentration	initial conformation	simulation time				total simulation time
		$CaCl_2$	KCl	$MgCl_2$	NaCl	
0 M	coil	N/A	N/A	N/A	N/A	4 μs
0 M	β	N/A	N/A	N/A	N/A	2.205 μs
0.1 M	coil	4 μs	4 μs	4 μs	4 μs	16 μs
0.1 M	β	2.924 μs	2.962 μs	3.489 μs	2.388 μs	11.76 μs
0.2 M	coil	4 μs	4 μs	4 μs	4 μs	16 μs
0.2 M	β	2.323 μs	2.440 μs	2.982 μs	2.07 μs	9.82 μs
0.3 M	coil	4 μs	4 μs	4 μs	4 μs	16 μs
0.3 M	β	2.568 μs	2.958 μs	2.633 μs	1.571 μs	9.73 μs
0.4 M	coil	4 μs	4 μs	4 μs	4 μs	16 μs
0.4 M	β	3.515 μs	3.985 μs	3.650 μs	2.250 μs	13.4 μs
0.5 M	coil	4 μs	4 μs	4 μs	4 μs	16 μs
0.5 M	β	2.711 μs	2.89 μs	2.8 μs	2.42 μs	10.82 μs

[a]The total simulation time for trajectories starting from a pre-formed β hairpin varied according to the breaking time of the hairpin.

the β structures were also computed using an autocorrelation function method (see below).

Trajectories using pure water environments (0 M) were prepared using the same methodology as the one with coil initial conditions with the exception of only adding one Na^+ ion to produce a charge-neutral system. 0 M trajectories were used to establish baseline measurements and to compare with previous work[36] that made use of the TIP4P water model. For each salt concentration and initial conformation, 10 independent production-run trajectories were generated. For the random coil initial condition trajectories, a total running time per trajectory was chosen to be 400 ns. Thus, for each random coil initial condition and salt concentration, a total of 4 μs of simulation time was generated. Additionally, 10 trajectories of pure water simulations for random coil initial conditions were also produced with a running time for each trajectory of 400 ns. The total running time for all of the random coil initial condition trajectories was 84 μs, and along with ~58 μs of simulation data from the preformed β-hairpins, the work presented here amounted to a total of ~142 μs (see Table 2).

It should be noted that one of the original goals of this study was to test the salts in the same TIP4P water model used in previous work[36,42] to allow for a direct comparison. However, during preliminary simulations, it was found that the decapeptide and $CaCl_2$ exhibited unphysical behavior (aggregation of cations along the peptide) when the TIP4P water model was used. To avoid this, the TIP3P water model was chosen instead, since it had been shown not to exhibit this anomaly under conditions similar to the ones used in our present work.[61,62]

Secondary Structure Classification. To determine the secondary structure per amino acid residue of Aβ_{21-30}, we used the STRIDE classification scheme.[63,64] Under this classification, individual amino acid residues were cast into one of the following secondary structure categories: coil (C), extended (E), bridge (B), turn (T), 3−10 helix (G), alpha-helix (H), or pi-helix (I). The secondary structure for a series of residues was then represented as a string of letters following the classifications listed above. Previous work[39] showed that the structure of the Aβ_{21-30} could be described by three general single-type families, as opposed to one per amino acid: loop1/turn, loop2/β-(hairpin/bridge), open/coil. In a similar fashion, here we used our STRIDE classifications to define four single-type families consisting of β-hairpin/bridge, turn, helix, or coil conformations. Although these families were structurally similar to those used in previous work, our new definitions offered computational advantages when calculating propensities and lifetimes. In our current scheme, β secondary structures were defined as any combination of two or more STRIDE bridge (B) or extended (E) classifications separated by at least one residue. For instance, the sequences CEECTTEECC and CBETTTBEBC were classified as β. We note that β structures under this classification were typically β-turns/β-hairpins due to the shortness of the Aβ_{21-30} monomer. The helix classification was defined as three or more adjacent H/G/I STRIDE labeled residues not previously classified as β structures (e.g., CHHHCCCTTC). Turns were defined as structures not belonging to either a helix or a β classification while having a STRIDE sequence that corresponded to a β or helix with T substitutions for all of the E/B/G/H/I residues. Coil structures were defined as any structure that did not fit into any of the previous classifications. Using the above classifications, the secondary structure for the decapeptide was separately determined at each simulation step as one of our four categories. An important note is that, because β-turns/β-hairpins are well-defined structural motifs, various results on β structures presented here were directly comparable to those found previously.[42,43] However, because all turns were classified as one single species, dynamical properties such as turn lifetimes were not directly comparable to previous findings where lifetimes were characterized only for subgroups of turn conformations determined by clustering of their mutual RMSD distances.[42]

Secondary Structure Distributions and Lifetimes. The time series of the secondary structure was used to compute the average number of frames in which the decapeptide existed in each of the secondary structure classifications described above. The result of these measurements when performed over each independent trajectory was a set of secondary structure propensity distributions for each concentration and initial condition.

Secondary structure lifetimes for each salt concentration and initial condition were obtained by decomposing the secondary structure time series for each trajectory into sets of four binary series, one for each secondary structure, and computing an autocorrelation function, with a maximum lag (where lag is defined as the number of skipped frames between correlation computations) equal to a quarter of the length of the trajectory, for each trajectory. The computed autocorrelation functions were then truncated at the first zero crossing or region of

dx.doi.org/10.1021/jp312653h | J. Phys. Chem. B 2013, 117, 6614−6624

negative curvature and fit to a decreasing exponential function $\exp(-t/\tau)$ with the secondary structure lifetime given by multiplying the frame saving rate (4 ps) by τ.

Hydrogen Bonds. Intrapeptide HBs were measured using the VMD[65] software package. We used a distance cutoff of 3 Å and a bonding angle of 20° between hydrogen donor−acceptor pairs in our definition of a HB. The average number of total HB events in a frame, specific salt-bridge events per frame between oppositely charged residues, and specific HBs between Asp23−Ser26/Asn27 were also measured, and are reported below.

Salt−Decapeptide Interactions. Interactions between the dissolved salt ions and Aβ_{21-30} were broken into two categories: direct and indirect interactions. Direct interactions were defined as those between the peptide and the dissolved salts through the formation of ion−residue contacts. Water mediated interactions were defined as modifications to the hydration behavior of the decapeptide due to interactions between the salts and the water.

(a). Direct Salt−Decapeptide Interactions. Ion−residue contacts were defined as the overlap between the solvation shell of the salt ion and an amino acid residue. The size of the solvation shell of each ion varied depending on the salt being considered and was defined to be equivalent to the second peak of the empirical radial distribution of the waters centered on the dissolved salt ions. These radial distribution functions were separately obtained by performing short (<100 ns) simulations for each salt in water (without the decapeptide) under the same conditions as the production runs, and then measuring the radial distribution function of the solvent with respect to the dissolved ions. Table 3 gives the measured values of the solvation shells.

Table 3. Size of Salt-Ion Solvation Shells

salt species	shell radius (Å)
Ca^{2+}	3.06
Mg^{2+}	2.68
K^{+}	3.3
Na^{+}	3.04
Cl^{-}	3.3

(b). Water Mediated Interactions. To determine the extent of water mediated interactions, we measured the mean residence time of water molecules belonging to the decapeptide's hydration shell (taken to be all water molecules within 5 Å of the decapeptide) and water−decapeptide HB formation for each environment. In order to obtain the measure of mean hydration shell water residence times, the following three-step calculation was performed: (i) construction of a list of all waters within the hydration shell at each time step, (ii) measurement of individual hydration water event lifetimes, and (iii) calculation of the mean of these lifetimes. To build the necessary time-dependent list of hydration shell water molecules, a search for water molecules fitting the hydration shell criterion was performed. Identified water molecules were then recorded by unique identification numbers. Once the list was constructed, equally spaced starting locations along the decapeptide's trajectories were selected and water lifetime events were recorded. To reduce fluctuations, waters that wandered farther than 5 Å from the hydration shell were still considered part of the shell for up to 16 ps, after which they would be deleted from the hydration-shell list or were kept depending on whether they met the distance criteria at that time. The mean water lifetime was then computed by averaging the individual water lifetimes but using a time cutoff of 8 ns to exclude outlier water lifetimes due to possible caging effects.

The mean water−decapeptide HBs per frame were measured by counting all water−decapeptide HBs at each frame and dividing by the total amount of frames. For convenience, this calculation was performed using the "g_hbond" tool from the GROMACS package instead of VMD.

RESULTS

In the following, measurements of the Aβ_{21-30}'s average secondary structure distributions, intrapeptide HB and salt-bridge formation, and secondary structure lifetimes are presented to show the contrast in the structural dynamics between pure water and the group IA/IIA chloride aqueous environments. Following this, ion−decapeptide contacts, hydration-shell residence times, and water−decapeptide HBs are presented to provide insight into the mechanisms of salt−decapeptide interactions.

Secondary Structure Propensity. Using our structure classification scheme (see Methods), we generated average secondary structure distributions for the Aβ_{21-30} decapeptide under our 0−0.5 M salt environments (Figure 1). From these

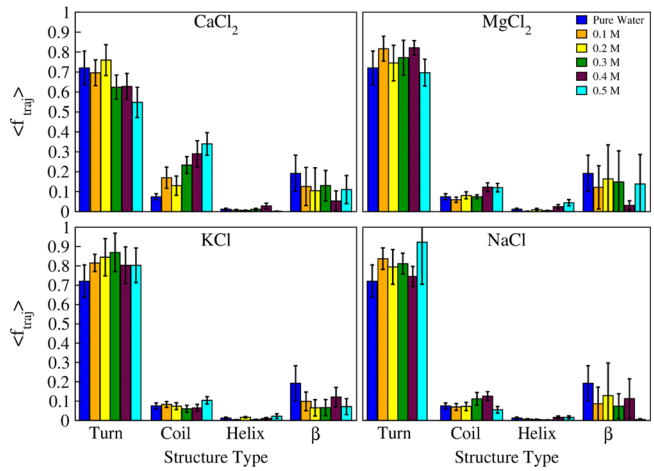

Figure 1. Mean fraction of trajectory time, $\langle f_{traj} \rangle$, exhibiting one of the defined secondary structures (turn, coil, helix, beta). Error bars were computed as the standard error of the mean over the course of all independent trajectories per concentration.

distributions, we found that for all concentrations turn secondary structures were the most predominant, followed by coil, β, and helix structures. This order of predominance (from high to low: turn, coil, and β structures), and in particular in the 0 M environment, was consistent with previous work on the decapeptide (and fragments containing the decapeptide).[36,37,39,43]

As a function of salt concentration, helix and β structures in both group IA and IIA environments did not show any significant change. On the other hand, turn and coil structure propensities in some salts exhibited changes as a function of concentration. In group IIA environments, coil propensities significantly increased as compared to the 0 M environment, while turn significantly decreased only in the $CaCl_2$ salt environment. Group IA environments did not exhibit significant changes in secondary structure propensities as a function of concentration or salt type.

dx.doi.org/10.1021/jp312653h | J. Phys. Chem. B 2013, 117, 6614−6624

Hydrogen Bonds and Salt Bridges. To investigate the possibility of subtle changes in structure not shown in the secondary structure analysis, changes in the prevalence of intrapeptide HBs were assessed by calculating the mean number of HBs per frame (Figure 2). In group IA, we found

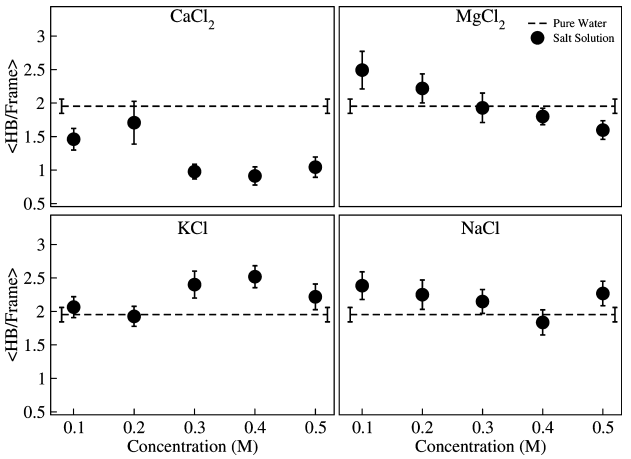

Figure 2. Average number of intrapeptide HBs per frame as a function of ionic concentration. Dashed horizontal lines correspond to results obtained from pure water environments. Error bars were calculated as the standard error of the mean from the measurements over individual trajectories.

that in KCl environments the mean number of HBs per frame for concentrations between 0.3 and 0.5 M remained consistently above the same measure of the 0 M (pure water) environments, although a significant trend with concentration did not exist. NaCl environments, however, had no significant increase or decrease in HBs per frame with concentration. In group IIA, $CaCl_2$ environments showed a significant decrease in the number of HBs per frame compared to 0 M environments at almost all concentrations, with the greatest decrease at concentrations greater than or equal to 0.3 M. $MgCl_2$ environments, unlike the other salt environments, showed a steady decrease in the mean number of HBs per frame with concentration with the highest and lowest values bracketing those of the 0 M environment.

Previous work[13,30,35−37,40−43] on the decapeptide (and fragments containing the decapeptide) showed that HBs between Asp23 and other amino acids and the formation of SB were important to the dynamics of the decapeptide. To determine any changes to specific intrapeptide HBs within the salt environments, we analyzed the formation of the Asp23−Ser26/Asn27 HBs and the Glu22/Asp23−Lys28 salt bridges. These data are presented in Figure 3 in terms of the mean specific HBs per frame. This figure shows that in most cases the occurrence of the Glu22/Asp23 and Lys28 salt-bridges and HBs between Asp23−Ser26/Asn27 were equal or greater than those for the 0 M environments for all salts, with the increases for these HBs following the trend KCl ∼ NaCl > $MgCl_2$ > $CaCl_2$, with KCl/NaCl having the largest increases and $CaCl_2$ having the smallest. Other salient features of this figure are that, for concentrations greater than or equal to 0.3 M, group IIA salts had the lowest Glu22−Lys28 salt-bridges per frame, with $CaCl_2$ having the lowest of the two. For the concentrations of 0.3−0.5 M, group IA salts had in general more HBs per frame and NaCl in particular was found to have an increasing trend of Asp23−Ser26/Asn27 HBs per frame.

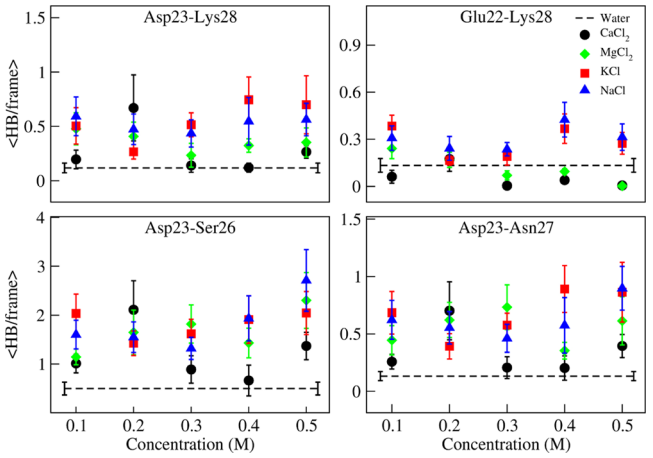

Figure 3. Average number of HBs per frame as a function of ionic concentration, where the HBs are between the Asp23−Lys28, Glu22−Lys28 (salt-bridges), and any two donor−acceptor atoms between Asp23−Ser26 and Asp23−Asn27. The horizontal dashed line corresponds to a pure water environment. Error bars were calculated as the standard error of the mean for each trajectory per concentration.

Structure Lifetimes. By definition, the mean secondary structure and hydrogen-bond/salt-bridge measurements presented above are averages over time. To examine details pertaining to the temporal evolution of particular structures of the decapeptide, such as long-lived motifs, we calculated secondary structure lifetimes (see Methods) and presented them in Figure 4. From this figure, we found that turn lifetimes

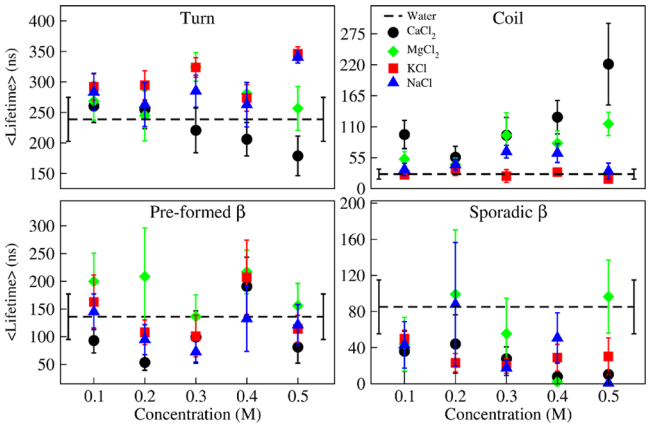

Figure 4. Average secondary structure lifetimes for turns, coils, and β-hairpins as a function of ionic concentration. The horizontal dashed line corresponds to a pure water environment. Error bars were calculated as the standard error of the mean for each trajectory per concentration.

decreased with increasing concentrations of $CaCl_2$ salts. However, turn structure lifetimes were found to be higher in both KCl and NaCl environments, with KCl having the largest increase. All of these turn structure lifetimes were substantially larger than those reported elsewhere[42] because here turns were considered as a single species while in previous work lifetimes were calculated for subgroups of turn structures defined by their RMSD distances. The lifetimes of coil structures in the $CaCl_2$ showed the opposite effect to the turns, and in general, group IIA salts at concentrations at 0.3 M and above showed increased lifetimes compared to all other tested environments.

dx.doi.org/10.1021/jp312653h | J. Phys. Chem. B 2013, 117, 6614−6624

However, the increase in the coil lifetimes in the $CaCl_2$ followed an increasing trend with concentration, while $MgCl_2$'s increase was mostly flat between 0.3 and 0.5 M. Under the group IA environments, there were no significant changes to the coil structure lifetimes when compared to the 0 M environments.

Lifetimes of the sporadically occurring β structure (Figure 4, lower right) showed a lower value than the 0 M for nearly all salt environments. However, because of the rarity in the occurrence of sporadically formed β-hairpin structures, these lifetime calculations were recalculated under a different scheme. This new scheme followed the methodology from previous work[42] and calculated lifetimes of preformed β_{28} hairpins, where additional trajectories (see Methods) were generated that started from a preformed β_{28} hairpin and lifetimes were obtained as described above (Figure 4, lower left). From these additional simulations, we found no significant changes to the lifetimes of preformed β structures regardless of the concentration and species of our salts.

Interaction Mechanisms. To investigate possible interaction mechanisms responsible for the changes to $A\beta_{21-30}$'s secondary structure, hydrogen-bond/salt-bridge formation, and dynamics compared to the 0 M environments, we examined direct salt−decapeptide interactions by measuring residue−ion contacts and water mediated interactions by measuring water−decapeptide HBs and hydration-shell water lifetimes. The residue−ion contacts were of interest, as they may have been involved in the screening of charged residue interactions and in the prevention or weakening of intrapeptide HB formation, while alterations to the formation of decapeptide−water HBs and hydration-shell water lifetimes may be indicative of changes to hydrophobic/hydrophilic interactions along the decapeptide induced by salt−water interactions.

Residue−Ion Contacts. Measurement of residue−ion contacts was performed by computing the average number of contacts per frame between the cationic and anionic species of the salts with any particular residue under each salt environment. Figure 5 shows that Ca^{2+} cations had a high average number of direct contact interactions relative to all of the other cation species, and a particularly high affinity for making contacts with the Glu22, Asp23, and Ala30. Interestingly,

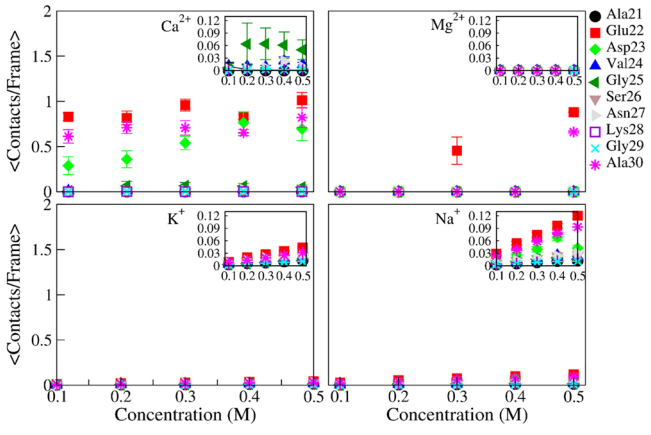

Figure 5. Mean number of contacts between the second solvation shell of cations and specified amino acids per frame for all concentrations. Error bars were calculated as the standard error of the mean from all trajectories per concentration. In most cases, the error bars were equal or smaller than the size of the symbol.

Asp23−Ca^{2+} contacts were found to increase with concentration, while Glu22/Ala30−Ca^{2+} contacts were approximately constant. Mg^{2+} cations also demonstrated a high affinity for contacts but only at concentrations of 0.3 and 0.5 M with Glu22. As the size of the Mg^{2+} cations was substantially smaller than those of the other three cations, we repeated these measurements, making use of Mg^{2+}'s third solvation shell (see Figure S3, Supporting Information) and found that Mg^{2+} does display Glu22 contacts at 0.4 M, suggesting that the anomalous lack of contacts at 0.4 M shown at the second solvation shell may be an artifact of narrow cutoffs. In the group IA cations, although there was a linear increase in average numbers of contacts with Glu22 and Asp23, the contact values for any residue were below ~0.06 and ~0.12 contacts per frame for K^+ and Na^+ (much lower than in the group IIA cations), respectively.

When measuring the anion−residue contacts (Figure 6), it was found that, irrespective of the cationic species in the

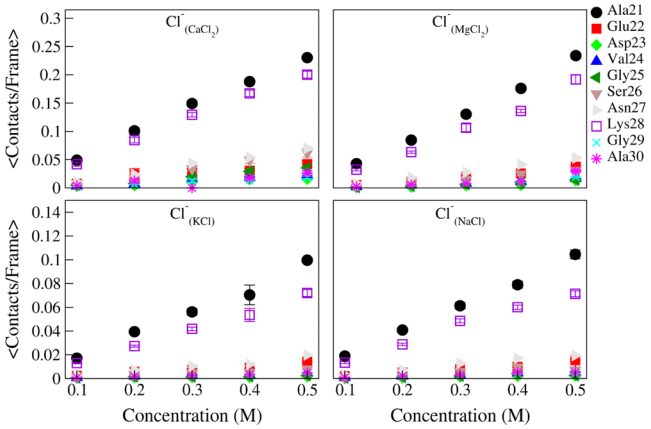

Figure 6. Mean number of contacts between the second solvation shell of Cl^- anions and specified amino acids per frame for all concentrations. Error bars were calculated as the standard error of the mean from all trajectories per concentration. In most cases, the error bars were equal or smaller than the size of the symbol.

environment, the Cl^- and Ala21/Lys28 contacts increased linearly with concentration, similar to that of the cation−residue contacts of group IA (Figure 5). It should be noted that the rate of increase of the Cl^- contacts for group IA conditions was nearly half of that for the group IIA ions, which we attributed to the doubled amount of anions necessary to balance the charges of the group IIA cations. The similar tendencies of interactions between all salts in Figure 6 demonstrated that the Cl^- ions did not introduce differential effects in each salt but rather acted as inert charge-neutralizing agents.

Water-Mediated Salt Interactions. As the structure of bulk water has been found in previous work to be largely unaffected by the addition of salts (see refs 66−68 and the review by Zhang and Cremer[69]), we chose to search for salt-specific changes in the hydration shell around the decapeptide that would indicate water-mediated interactions between ions and the decapeptide. To gauge these interactions, we calculated changes in the dynamics of the water molecules forming the decapeptide's hydration shell as a function of ion concentration. These changes in the dynamics were quantified by measuring the mean residence time of the water molecules in the hydration shell, as described in the Methods section, and the

dx.doi.org/10.1021/jp312653h | J. Phys. Chem. B 2013, 117, 6614−6624

mean number of HBs between the decapeptide and the water per frame. Figure 7 shows the mean hydration-shell water

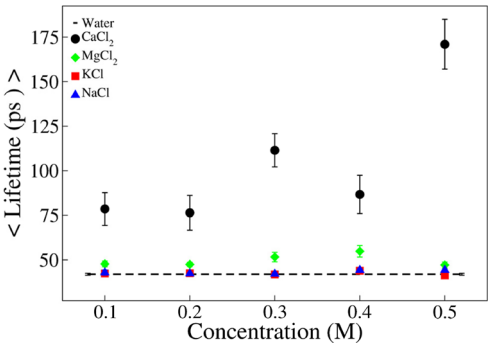

Figure 7. Mean residence time of water molecules in the hydration shell as a function of ionic concentration for all salts. The horizontal dashed line corresponds to a pure water environment. Error bars were calculated as the standard error of the mean for each trajectory per concentration.

residence times vs concentration for all of our tested salt environments. The data presented in this figure shows that the group IA salts, regardless of concentration, had no significant effect on the lifetime of the hydration shell water molecules. On the other hand, group IIA environments had significant increases in the lifetime with increasing concentration, with hydration shell lifetimes significantly higher for $CaCl_2$ than those measured from the $MgCl_2$ environments.

Average HBs between the decapeptide and water, $\langle HB_{WP} \rangle$, were calculated and are shown in Figure 8. In this figure, results

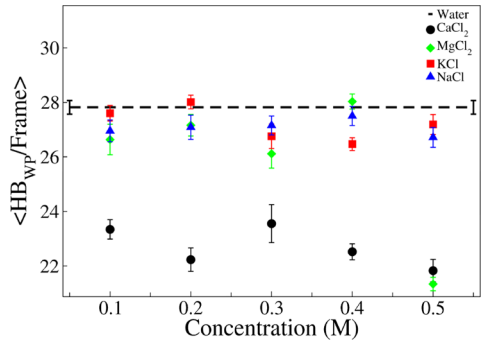

Figure 8. Water−decapeptide HBs per frame as a function of ionic concentration. The horizontal dashed line corresponds to a 0 M (pure water) environment. Error bars were calculated as the standard error of the mean for each trajectory per concentration.

for group IA salts show that KCl and NaCl environments had a negligible effect on the HB network, although the total number of contacts was in general slightly lower than that for the pure water environment. For the group IIA environments, $CaCl_2$ was shown to substantially decrease the formation of water−peptide HBs for all concentrations, with $MgCl_2$ having a similar effect but only at high (0.5 M) concentrations.

DISCUSSION

Previous computational and experimental work has focused on the structure and dynamics of the Aβ_{21-30} but only under pure water environments.[36,37,40−43] Here, we investigated, using all-atom explicit solvent molecular dynamics simulations, the influence of neurobiologically relevant salts on the dynamics of the Aβ_{21-30} decapeptide. We found that propensities and lifetimes of the decapeptide's turn and coil structures were influenced by both group IA and IIA environments, with group IIA environments significantly increasing coil propensities and lifetimes and in particular $CaCl_2$ decreasing turn propensities, and group IA having a significant increase to the lifetimes of turn structures. We also found that the lifetimes of β secondary structures were not affected by the salts tested here when compared with previous simulations using pure water environments. In addition, Asp23−Ser26/Asn27 HBs and the Glu22/Asp23−Lys28 salt bridges were in general increased by group IA salts relative to group IIA and 0 M environments. $CaCl_2$ environments were found to have additional effects by showing a decreased amount of intrapeptide HBs, the highest ion−peptide rate of contacts, the longest lifetime of hydration-shell water molecules, and the lowest amount of HBs between the decapeptide and water.

Overall, our data indicated that the tested salts had varying degrees of influence on the distribution of HBs and contacts in the Aβ_{21-30}. Increased amounts of the Glu22/Asp23 and Lys28 salt-bridges and HBs between Asp23−Ser26/Asn27 in the group IA salts shown in Figure 3, and the lower values in their total decapeptide−water HBs shown in Figure 8, were consistent with ion−water interactions that tended to decrease the number of available water molecules that could form HBs with the decapeptide, thus inducing the decapeptide to increase intrapeptide HBs. Interestingly, these increased amounts of intrapeptide HBs, and in particular the Asp23−Ser26 HB previously correlated with the formation of turns,[37,40,42,70,71] did not influence the amounts of secondary structure presented here with these salts. Group IIA salts were more complex, displaying salt-bridges in line with values of the 0 M environment and intermediate numbers of Asp23−Ser26/Asn27 HBs while at the same time exhibiting the lowest numbers of decapeptide−water HBs. In this case, the lower number of salt-bridges was consistent with the observed high number of direct ion−decapeptide contacts in which cation−Glu22 or cation−Asp23 replaced salt-bridges, while cation−Ala30 reduced the number of decapeptide−water HBs. The high number of these direct contacts in the $CaCl_2$ was also consistent with the lowest Asp23−Ser26/Asn27 HBs that correlated with a significant reduction of turn structure.

Dynamical properties were also different between group IA and IIA salts, in particular turn and coil lifetimes. Before examining the details, however, it is important to note that the structural lifetimes reported here were a measure of the characteristic time that the decapeptide existed uninterrupted in a particular secondary structure. In this work, we chose to define four secondary structures, of which the turn was defined as a single group of conformations. Because in previous work we defined different types of turns by a RMSD distance cutoff (1 Å) instead of a single structural species,[42] previous lifetimes (∼15 ns) were smaller than those calculated here (∼200 ns). The current definition has the advantage that turns are uniquely defined, since clustering by RMSD can result in widely differing populations of turn clusters when changing RMSD by only slight amounts.[42] However, our current definition of lifetimes allows for a very wide variability in structure (mutual RMSDs of more than 4 Å) and does not imply duration of any persistent turn structure.

Group IA turn lifetimes were significantly higher than those for the group IIA and the 0 M environment, while coil lifetimes were not different than the 0 M. On the other hand, turn

dx.doi.org/10.1021/jp312653h | J. Phys. Chem. B 2013, 117, 6614−6624

lifetimes in group IIA were either similar to the 0 M (Mg^{2+}) or decreasing (Ca^{2+}), while coil lifetimes were significantly increasing with concentration. The ion-dependent mechanism responsible for the high turn lifetimes, higher frequency of intrapeptide HBs, and slightly lower water−decapeptide HBs in the group IA salts was not clear, since in these salts there were no substantial decapeptide−ion contacts. Also, screening effects (Debye−Hückel screening) by the ions were found not to be relevant as the number of salt-bridges were either unchanged or higher as compared to the 0 M environment (screening would have decreased these salt-bridges). Additional measurements of the mean residence time of water molecules in the hydration shell (Figure 7) and the rotational autocorrelation time constants of water molecules (Figure S4, Supporting Information) found no changes between 0 M conditions and the group IA environments. Also, an analysis of compactness of structures did not show a conclusive result where the radius of gyration of turn conformations (Figures S5 and S6, Supporting Information) showed an increased compactness in the group IA not present in the $CaCl_2$ but present in $MgCl_2$ salt environments at low concentration (<0.3 M). These data then suggest that, although the exact mechanism behind the high turn lifetimes in the group IA salt environments is unknown, it is significantly weaker and independent of ion−residue contacts and the solvent interactions examined in this work. The determination of this mechanism is the focus of ongoing work.

In the dynamics of the group IIA salt environments, the low or decreased lifetimes of turns and the high coil lifetimes could be attributed to the high number of direct decapeptide−ion contacts. As outlined above, the high number of these contacts also correlated with the decrease in the Asp23−Ser26/Asn27 HBs and the decrease in the number of water−decapeptide and salt-bridges. Although this decapeptide−ion mechanism did not appear to apply to the Mg^{2+}, when extending the definition of contacts to the third solvation shell, we found that the number of contacts in the Mg^{2+}, though still reduced, mirrored the behavior found in Ca^{2+}. Regarding the dynamics of the hydration-shell waters, the group IIA salts showed in general higher mean water residence times than the group IA which were not different than in the 0 M environment. This increase was not expected, since cation−residue contacts were expected to increase the diffusion of the hydration-shell waters by diminishing the formation of water−peptide HBs. We attributed this effect to electrostatic interactions between the divalent cations near the decapeptide and the hydration-shell water molecules that slowed the motion of the hydration shell water molecules. In the $CaCl_2$ environments, this slowing down of these water molecules was also found to be consistent with the observed decrease of turn propensities and lifetimes. In this scheme, the slowed motion of the hydration-shell waters hindered the formation of turns by hampering coils from expelling the excess hydration-shell water molecules from within the center of the decapeptide. This resulted in an effective increase in the free energy of the turn that extended and decreased lifetimes for coil and turn structures, respectively. This mechanism was also consistent with the trends found in the $MgCl_2$, although the effects were much smaller.

By examining the changes in all of the properties analyzed here, specifically at the high salt concentrations, we rank the salts by their effective "influence" in the decapeptide behavior. In particular, ranking the salts by increasing coil lifetimes or mean hydration-shell residence times, we obtained the following series: $CaCl_2$ > $MgCl_2$> NaCl ∼ KCl. Very similar is also the ranking by number of direct decapeptide−ion contacts: $CaCl_2$ > $MgCl_2$> NaCl > KCl. Performing a similar ranking in terms of increasing turn lifetimes gave the following: $CaCl_2$ < $MgCl_2$ < NaCl < KCl. By ranking the salts based on their ability to increase intrapeptide HBs and by their turn propensity, we obtain a similar ranking: $CaCl_2$ < $MgCl_2$ < KCl ∼ NaCl, which also applies to the total intrapeptide HBs. Finally, by ranking in order of coil propensity, we obtain the following: $CaCl_2$ > $MgCl_2$ > KCl > NaCl. All of these rankings clearly state that: (i) group IIA salts have more "influence" than group IA salts on the behavior of the decapeptide and (ii) within groups, the Ca^{2+} is more influential than the Mg^{2+} and the Na^+ and K^+ are at roughly equal standing to each other.

It is instructive to compare our current results on the behavior of the $A\beta_{21-30}$ monomer with experimental studies of the aggregation of full-length Aβ, although conclusions can only be speculative at this point. However, parallels can be made between them. For example, Klement et al.[46] subjected full length Aβ peptides to a variety of salt environments and measured changes to the aggregation of the peptide. Their results on KCl, NaCl, and $MgCl_2$ environments with concentrations between 0 and 0.5 M resulted in a ranking of decreasing aggregation of Mg^{2+} > Na^+ > K^+. Similar to this work, Issacs et al.[49] reported measurements on enhanced aggregation by $CaCl_2$ at concentrations much smaller than the extracellular *in vivo* concentration of 0.002 M. By considering both of these results, we can construct an experimental ranking of salt "influence" on Aβ as $CaCl_2$ ≥ $MgCl_2$ > KCl > NaCl, where the $CaCl_2$ is positioned first on the basis of the high sensitivity of aggregation to the very small $CaCl_2$ concentration. The close similarity between this ranking and the one found here suggests that the physical properties of ions may play an important role in the structure and dynamics of the Aβ while their increasing concentration may affect aggregation pathways.

Similarities aside, one important point has to be made regarding the difference between the ranking found here and the one found in the literature in the placement of $MgCl_2$ relative to the $CaCl_2$ and KCl. Here we found that the $CaCl_2$ was significantly more influential than the $MgCl_2$, with $MgCl_2$ having an "influence" strength closer to KCl. Experiments showed, however, that $CaCl_2$ and $MgCl_2$ could (at times) be found at an equivalent level of influence where their roles could be interchanged. Additionally, KCl was shown to be significantly less influential than $MgCl_2$. It is possible that this difference has its roots at a possible incorrect parametrization of the Mg^{2+} cation as noted by Mamatkulov[72] for the AMBER, CHARMM, and GROMOS force fields. This problem could also be responsible for the sudden drop in the Mg^{2+}−water radial distribution function after the first water-shell peak (data not shown) that could in principle cage waters for an abnormally high amount of time, thus artificially increasing the binding interactions between ion and water (see Figure S4, Supporting Information) and thus lessening Mg^{2+}−decapeptide effects. However, our preliminary tests using the OPLS-AA force field with the Mg^{2+} cation yielded similar hydration-shell sizes for the Mg^{2+} cations as those obtained by Mamatkulov after their improved parametrization. Nonetheless, it is still an open question whether the OPLS-AA force field parameters take full account of the influence of the Mg^{2+}.

In sum, we have shown that neurobiologically important group IA and IIA salts introduce important changes to the structure and dynamics of the $A\beta_{21-30}$ decapeptide relative to

dx.doi.org/10.1021/jp312653h | J. Phys. Chem. B 2013, 117, 6614−6624

bulk nonionic environments. In particular, Ca^{2+} was shown to act as a HB and turn destabilizing agent of $A\beta_{21-30}$ through the occurrence of peptide−ion contact interactions and alterations to the decapeptide's hydration shell, while group IA salts increased intrapeptide HBs and turn lifetimes. These conclusions may be of importance in understanding the early stages of aggregation of the full-length Aβ, as the enhanced propensity of open structures under certain, but not all, salt environments could provide additional interpeptide contact sites promoting aggregation and may help understand the experimental observation of increased aggregation rates under similar salt environments.[46−50] The presented cation-residue/water-mediated interaction mechanism and salt-induced modifications to the peptide's structure and dynamics may help in our understanding of the complex interactions existing in the *in vivo* environment and may lead to advances in prevention and treatment of Alzheimer's disease.

■ ASSOCIATED CONTENT

Supporting Information

Information on time step and cutoff selections used in our simulations, along with additional supporting measurements discussed in the text. This material is available free of charge via the Internet at http://pubs.acs.org.

■ AUTHOR INFORMATION

Corresponding Author

*Phone: 215-895-2739. E-mail: ccruz@drexel.edu.

Notes

The authors declare no competing financial interest.

■ ACKNOWLEDGMENTS

Computational time was provided in part by XSEDE computational resources grant TG-MCB110142.

■ ABBREVIATIONS:

Aβ, amyloid β-protein; AD, Alzheimer's disease; HB, hydrogen bond; MD, molecular dynamics; SB, salt bridge

■ REFERENCES

(1) Hardy, J.; Allsop, D. Amyloid Deposition as the Central Event in the Aetiology of Alzheimer's Disease. *Trends Pharmacol. Sci.* **1991**, *12*, 383−388.

(2) Hardy, J. A.; Higgins, G. A. Alzheimer's Disease: The Amyloid Cascade Hypothesis. *Science* **1992**, *256*, 184−185.

(3) Kirkitadze, M. D.; Bitan, G.; Teplow, D. B. Paradigm Shifts in Alzheimer's Disease and Other Neurodegenerative Disorders: the Emerging Role of Oligomeric Assemblies. *J. Neurosci. Res.* **2002**, *69*, 567−577.

(4) Walsh, D. M.; Klyubin, I.; Shankar, G. M.; Townsend, M.; Fadeeva, J. V.; Betts, V.; Podlisny, M. B.; Cleary, J. P.; Ashe, K. H.; Rowan, M. J.; et al. The Role of Cell-Derived Oligomers of ABeta in Alzheimer's Disease and Avenues for Therapeutic Intervention. *Biochem. Soc. Trans.* **2005**, *33*, 1087−1090.

(5) Klein, W. L.; Stine, W. B. J.; Teplow, D. B. Small Assemblies of Unmodified Amyloid Beta-Protein Are the Proximate Neurotoxin in Alzheimer's Disease. *Neurobiol. Aging* **2004**, *25*, 569−580.

(6) Haass, C.; Selkoe, D. J. Soluble Protein Oligomers in Neurodegeneration: Lessons from the Alzheimer's Amyloid Beta-Peptide. *Nat. Rev. Mol. Cell Biol.* **2007**, *8*, 101−112.

(7) Roychaudhuri, R.; Yang, M.; Hoshi, M. M.; Teplow, D. B. Amyloid Beta-Protein Assembly and Alzheimer Disease. *J. Biol. Chem.* **2009**, *284*, 4749−4753.

(8) Walsh, D. M.; Selkoe, D. J. ABeta Oligomers - A Decade of Discovery. *J. Neurochem.* **2007**, *101*, 1172−1184.

(9) Lesne, S.; Koh, M. T.; Kotilinek, L.; Kayed, R.; Glabe, C. G.; Yang, A.; Gallagher, M.; Ashe, K. H. A Specific Amyloid-Beta Protein Assembly in the Brain Impairs Memory. *Nature* **2006**, *440*, 352−357.

(10) Lambert, M. P.; Barlow, A. K.; Chromy, B. A.; Edwards, C.; Freed, R.; Liosatos, M.; Morgan, T. E.; Rozovsky, I.; Trommer, B.; Viola, K. L.; et al. Diffusible, Nonfibrillar Ligands Derived from Abeta1−42 Are Potent Central Nervous System. Neurotoxins. *Proc. Natl. Acad. Sci. U.S.A.* **1998**, *95*, 6448−6453.

(11) Teplow, D. B.; Lazo, N. D.; Bitan, G.; Bernstein, S.; Wyttenbach, T.; Bowers, M. T.; Baumketner, A.; Shea, J.; Urbanc, B.; Cruz, L.; et al. Elucidating Amyloid Beta Protein Folding and Assembly: A Multidisciplinary Approach. *Acc. Chem. Res.* **2006**, *39*, 635−645.

(12) Urbanc, B.; Cruz, L.; Yun, S.; Buldyrev, S. V.; Bitan, G.; Teplow, D. B.; Stanley, H. E. In Silico Study of Amyloid Beta-Protein Folding and Oligomerization. *Proc. Natl. Acad. Sci. U.S.A.* **2004**, *101*, 17345−17350.

(13) Urbanc, B.; Cruz, L.; Teplow, D. B.; Stanley, H. E. Computer Simulations of Alzheimer's Amyloid Beta-Protein Folding and Assembly. *Curr. Alzheimer Res.* **2006**, *3*, 493−504.

(14) Hamley, I. W. The Amyloid Beta Peptide: A Chemist's Perspective. Role in Alzheimer's and Fibrillization. *Chem. Rev.* **2012**, *112* (10), 5147−5192.

(15) Fink, A. L. Natively Unfolded Proteins. *Curr. Opin. Struct. Biol.* **2005**, *15*, 35−41.

(16) Uversky, V. N. Natively Unfolded Proteins: A Point Where Biology Waits for Physics. *Protein Sci.* **2002**, *11*, 739−756.

(17) Bitan, G.; Lomakin, A.; Teplow, D. B. Amyloid Beta-Protein Oligomerization: Prenucleation Interactions Revealed by Photo-Induced Cross-Linking of Unmodified Proteins. *J. Biol. Chem.* **2001**, *276*, 35176−35184.

(18) Teplow, D. B. Preparation of Amyloid β-Protein for Structural and Functional Studies. Amyloid, Prions, and Other Protein Aggregates, Pt C; Elsevier Academic Press Inc: San Diego, CA, 2006; Vol. *413*, p 20.

(19) Lee, J. P.; Stimson, E. R.; Ghilardi, J. R.; Mantyh, P. W.; Lu, Y. A.; Felix, A. M.; Llanos, W.; Behbin, A.; Cummings, M.; Van Criekinge, M.; et al. 1H NMR of A Beta Amyloid Peptide Congeners in Water Solution. Conformational Changes Correlate with Plaque Competence. *Biochemistry* **1995**, *34*, 5191−5200.

(20) Zhang, S.; Iwata, K.; Lachenmann, M. J.; Peng, J. W.; Li, S.; Stimson, E. R.; Lu, Y.; Felix, A. M.; Maggio, J. E.; Lee, J. P. The Alzheimer's Peptide A Beta Adopts a Collapsed Coil Structure in Water. *J. Struct. Biol.* **2000**, *130*, 130−141.

(21) Riek, R.; Guntert, P.; Dobeli, H.; Wipf, B.; Wuthrich, K. NMR Studies in Aqueous Solution Fail to Identify Significant Conformational Differences between the Monomeric Forms of Two Alzheimer Peptides with Widely Different Plaque-Competence, ABeta(1−40) and ABeta(1−42). *Eur. J. Biochem.* **2001**, *268*, 5930−5936.

(22) Hou, L.; Shao, H.; Zhang, Y.; Li, H.; Menon, N. K.; Neuhaus, E. B.; Brewer, J. M.; Byeon, I. L.; Ray, D. G.; Vitek, M. P.; et al. Solution NMR Studies of the ABeta(1−40) and ABeta(1−42) Peptides Establish That the Met35 Oxidation State Affects the Mechanism of Amyloid Formation. *J. Am. Chem. Soc.* **2004**, *126*, 1992−2005.

(23) Wei, G.; Shea, J. Effects of Solvent on the Structure of the Alzheimer Amyloid-Beta(25−35) Peptide. *Biophys. J.* **2006**, *91*, 1638−1647.

(24) Zanuy, D.; Ma, B.; Nussinov, R. Short Peptide Amyloid Organization: Stabilities and Conformations of the Islet Amyloid Peptide NFGAIL. *Biophys. J.* **2003**, *84*, 1884−1894.

(25) Klimov, D.; Thirumalai, D. Dissecting the Assembly of A Beta(16−22) Amyloid Peptides into Antiparallel Beta Sheets. *Structure* **2003**, *11*, 295−307.

(26) Favrin, G.; Irback, A.; Mohanty, S. Oligomerization of Amyloid Abeta16−22 Peptides Using Hydrogen Bonds and Hydrophobicity Forces. *Biophys. J.* **2004**, *87*, 3657−3664.

(27) Santini, S.; Wei, G.; Mousseau, N.; Derreumaux, P. Pathway Complexity of Alzheimer's Beta-Amyloid ABeta(16−22) Peptide Assembly. *Structure* **2004**, *12*, 1245−1255.
(28) Ma, B.; Nussinov, R. Stabilities and Conformations of Alzheimer's Beta-Amyloid Peptide Oligomers (ABeta 16−22, Abeta 16−35, and Abeta 10−35): Sequence Effects. *Proc. Natl. Acad. Sci. U.S.A.* **2002**, *99*, 14126−14131.
(29) Balbach, J. J.; Ishii, Y.; Antzutkin, O. N.; Leapman, R. D.; Rizzo, N. W.; Dyda, F.; Reed, J.; Tycko, R. Amyloid Fibril Formation by A Beta 16−22, A Seven-Residue Fragment of the Alzheimer's Beta-Amyloid Peptide, and Structural Characterization by Solid State NMR. *Biochem.* **2000**, *39*, 13748−13759.
(30) Baumketner, A.; Shea, J. The Structure of the Alzheimer Amyloid Beta 10−35 Peptide Probed through Replica-Exchange Molecular Dynamics Simulations in Explicit Solvent. *J. Mol. Biol.* **2007**, *366*, 275−285.
(31) Melquiond, A.; Dong, X.; Mousseau, N.; Derreumaux, P. Role of the Region 23−28 in ABeta Fibril Formation: Insights from Simulations of the Monomers and Dimers of Alzheimer's Peptides ABeta40 and Abeta42. *Curr. Alzheimer Res.* **2008**, *5*, 244−250.
(32) Baumketner, A.; Shea, J. Folding Landscapes of the Alzheimer Amyloid Beta(12−28). Peptide. *J. Mol. Biol.* **2006**, *362*, 567−579.
(33) Baumketner, A.; Krone, M. G.; Shea, J. Role of the Familial Dutch Mutation E22Q in the Folding and Aggregation of the 15−28 Fragment of the Alzheimer Amyloid-Beta Protein. *Proc. Natl. Acad. Sci. U.S.A* **2008**, *105*, 6027−6032.
(34) Chebaro, Y.; Mousseau, N.; Derreumaux, P. Structures and Thermodynamics of Alzheimer's Amyloid-Beta Abeta(16−35) Monomer and Dimer by Replica Exchange Molecular Dynamics Simulations: Implication for Full-Length Abeta Fibrillation. *J. Phys. Chem. B* **2009**, *113*, 7668−7675.
(35) Lazo, N. D.; Grant, M. A.; Condron, M. C.; Rigby, A. C.; Teplow, D. B. On the Nucleation of Amyloid Beta-Protein Monomer Folding. *Protein Sci.* **2005**, *14*, 1581−1596.
(36) Cruz, L.; Urbanc, B.; Borreguero, J. M.; Lazo, N. D.; Teplow, D. B.; Stanley, H. E. Solvent and Mutation Effects on the Nucleation of Amyloid Beta-Protein Folding. *Proc. Natl. Acad. Sci. U.S.A.* **2005**, *102*, 18258−18263.
(37) Baumketner, A.; Bernstein, S. L.; Wyttenbach, T.; Lazo, N. D.; Teplow, D. B.; Bowers, M. T.; Shea, J. Structure of the 21−30 Fragment of Amyloid Beta-Protein. *Protein Sci.* **2006**, *15*, 1239−1247.
(38) Borreguero, J. M.; Urbanc, B.; Lazo, N. D.; Buldyrev, S. V.; Teplow, D. B.; Stanley, H. E. Folding Events in the 21−30 Region of Amyloid Beta-Protein (ABeta) Studied in Silico. *Proc. Natl. Acad. Sci. U.S.A.* **2005**, *102*, 6015−6020.
(39) Chen, W.; Mousseau, N.; Derreumaux, P. The Conformations of the Amyloid-Beta(21−30) Fragment Can Be Described by Three Families in Solution. *J. Chem. Phys.* **2006**, *125* (8), 84911.
(40) Fawzi, N. L.; Phillips, A. H.; Ruscio, J. Z.; Doucleff, M.; Wemmer, D. E.; Head-Gordon, T. Structure and Dynamics of the Abeta(21−30) Peptide from the Interplay of NMR Experiments and Molecular Simulations. *J. Am. Chem. Soc.* **2008**, *130*, 6145−6158.
(41) Tarus, B.; Straub, J. E.; Thirumalai, D. Structures and Free-Energy Landscapes of the Wild Type and Mutants of the Abeta(21−30) Peptide Are Determined by an Interplay Between Intrapeptide Electrostatic and Hydrophobic Interactions. *J. Mol. Biol.* **2008**, *379*, 815−829.
(42) Cruz, L.; Rao, J. S.; Teplow, D. B.; Urbanc, B. Dynamics of Metastable Beta-Hairpin Structures in the Folding Nucleus of Amyloid Beta-Protein. *J. Phys. Chem. B* **2012**, *116*, 6311−6325.
(43) Rao, J. S.; Cruz, L. Effects of Confinement on the Structure and Dynamics of an Intrinsically Disordered Peptide: A Molecular-Dynamics Study. *J. Phys. Chem. B* **2013**, 3707−3719.
(44) Neira, J. L.; Fersht, A. R. An NMR Study on the Beta-Hairpin Region of Barnase. *Folding Des.* **1996**, *1*, 231−241.
(45) Selkoe, D. J. Alzheimer's Disease: Genes, Proteins, and Therapy. *Physiol. Rev.* **2001**, *81*, 741−766.
(46) Klement, K.; Wieligmann, K.; Meinhardt, J.; Hortschansky, P.; Richter, W.; Fandrich, M. Effect of Different Salt Ions on the Propensity of Aggregation and on the Structure of Alzheimer's Abeta(1−40) Amyloid Fibrils. *J. Mol. Biol.* **2007**, *373*, 1321−1333.
(47) Mithu, V. S.; Sarkar, B.; Bhowmik, D.; Chandrakesan, M.; Maiti, S.; Madhu, P. K. Zn(++) Binding Disrupts the Asp(23)-Lys(28) Salt Bridge without Altering the Hairpin-Shaped Cross-β Structure of Aβ(42) Amyloid Aggregates. *Biophys. J.* **2011**, *101*, 2825−2832.
(48) Itkin, A.; Dupres, V.; Dufrene, Y. F.; Bechinger, B.; Ruysschaert, J.; Raussens, V. Calcium Ions Promote Formation of Amyloid B-Peptide (1−40) Oligomers Causally Implicated in Neuronal Toxicity of Alzheimer's Disease. *PLoS One* **2011**, *6*, e18250.
(49) Isaacs, A. M.; Senn, D. B.; Yuan, M.; Shine, J. P.; Yankner, B. A. Acceleration of Amyloid Beta-Peptide Aggregation by Physiological Concentrations of Calcium. *J. Biol. Chem.* **2006**, *281*, 27916−27923.
(50) Garai, K.; Sengupta, P.; Sahoo, B.; Maiti, S. Selective Destabilization of Soluble Amyloid Beta Oligomers by Divalent Metal Ions. *Biochem. Biophys. Res. Commun.* **2006**, *345*, 210−215.
(51) Berendsen, H. J. C.; Van der Spoel, D.; Vandrunen, R. Gromacs-A Message-Passing Parallel Molecular Dynamics Implementation. *Comput. Phys. Commun.* **1995**, *91*, 43−56.
(52) Van der Spoel, D.; Lindahl, E.; Hess, B.; Groenhof, G.; Mark, A. E.; Berendsen, H. J. C. Gromacs: Fast, Flexible, and Free. *J. Comput. Chem.* **2005**, *26*, 1701−1718.
(53) Hess, B.; Kutzner, C.; Van der Spoel, D.; Lindahl, E. GROMACS 4: Algorithms for Highly Efficient, Load-Balanced, and Scalable Molecular Simulation. *J. Chem. Theory Comput.* **2008**, *4*, 435−447.
(54) Kaminski, G. A.; Friesner, R. A.; Tirado-Rives, J.; Jorgensen, W. L. Evaluation and Reparametrization of the OPLS-AA Force Field for Proteins via Comparison with Accurate Quantum Chemical Calculations on Peptides. *J. Phys. Chem. B* **2001**, *105*, 6474−6487.
(55) Jorgensen, W. L.; Maxwell, D. S.; Tirado-Rives, J. Development and Testing of the OPLS All-Atom Force Field on Conformational Energetics and Properties of Organic Liquids. *J. Am. Chem. Soc.* **1996**, *118*, 11225−11236.
(56) Jorgensen, W. L.; Chandrasekhar, J.; Madura, J. D.; Impey, R. W.; Klein, M. L. Comparison of Simple Potential Functions for Simulating Liquid Water. *J. Chem. Phys.* **1983**, *79*, 926−935.
(57) Mackerell, A.; Bashford, D.; Bellott, M.; Dunbrack, R.; Evanseck, J.; Field, M.; Fischer, S.; Gao, J.; Guo, H.; Ha, S.; et al. All-Atom Empirical Potential for Molecular Modeling and Dynamics Studies of Proteins. *J. Phys. Chem. B* **1998**, *102*, 3586−3616.
(58) Berendsen, H. J. C.; Postma, J. P. M.; Vangunsteren, W. F.; Dinola, A.; Haak, J. R. Molecular Dynamics with Coupling to an External Bath. *J. Chem. Phys.* **1984**, *81*, 3684−3690.
(59) Miyamoto, S.; Kollman, P. A. Settle: An Analytical Version of the SHAKE and RATTLE Algorithm for Rigid Water Models. *J. Comput. Chem.* **1992**, *13*, 952−962.
(60) Hess, B.; Bekker, H.; Berendsen, H. J. C.; Fraaije, J. G. E. M. LINCS: A Linear Constraint Solver for Molecular Simulations. *J. Comput. Chem.* **1997**, *18*, 1463−1472.
(61) Florova, P.; Sklenovsky, P.; Banas, P.; Otyepka, M. Explicit Water Models Affect the Specific Solvation and Dynamics of Unfolded Peptides while the Conformational Behavior and Flexibility of Folded Peptides Remain Intact. *J. Chem. Theory Comput.* **2010**, *6*, 3569−3579.
(62) Sgourakis, N. G.; Yan, Y.; Mccallum, S. A.; Wang, C.; Garcia, A. E. The Alzheimer's Peptides Abeta40 and 42 Adopt Distinct Conformations in Water: A Combined MD/NMR Study. *J. Mol. Biol.* **2007**, *368*, 1448−1457.
(63) Heinig, M.; Frishman, D. STRIDE: A Web Server for Secondary Structure Assignment from Known Atomic Coordinates of Proteins. *Nucleic Acids Res.* **2004**, *32*, 500−502.
(64) Frishman, D.; Argos, P. Knowledge-Based Protein Secondary Structure Assignment. *Proteins: Struct., Funct., Genet.* **1995**, *23*, 566−579.
(65) Humphrey, W.; Dalke, A.; Schulten, K. VMD: Visual Molecular Dynamics. *J. Mol. Graphics* **1996**, *14*, 33−38.
(66) Omta, A. W.; Kropman, M. F.; Woutersen, S.; Bakker, H. J. Negligible Effect of Ions on the Hydrogen-Bond Structure in Liquid Water. *Science* **2003**, *301*, 347−349.

(67) Kropman, M. F.; Bakker, H. J. Effect of Ions on the Vibrational Relaxation of Liquid Water. *J. Am. Chem. Soc.* **2004**, *126*, 9135−9141.
(68) Batchelor, J. D.; Olteanu, A.; Tripathy, A.; Pielak, G. J. Impact of Protein Denaturants and Stabilizers on Water Structure. *J. Am. Chem. Soc.* **2004**, *126*, 1958−1961.
(69) Zhang, Y.; Cremer, P. S. Interactions between Macromolecules and Ions: the Hofmeister Series. *Curr. Opin. Chem. Biol.* **2006**, *10*, 658−663.
(70) Krone, M. G.; Baumketner, A.; Bernstein, S. L.; Wyttenbach, T.; Lazo, N. D.; Teplow, T. B.; Bowers, M. T.; Shea, J. Effects of Familiar Alzheimer's Disease Mutations on the Folding Nucleation of Amyloid *β*-Protein. *J. Mol. Biol.* **2008**, *381*, 221−228.
(71) Ball, K. A.; Phillips, A. H.; Nerenberg, P. S.; Fawzi, N. L.; Wemmer, D. E.; Head-Gordon, T. Homogeneous and Heterogeneous Tertiary Structure Ensembles of Amyloid-*β* Peptides. *Biochemistry* **2011**, *50*, 7612−7628.
(72) Mamatkulov, S.; Fyta, M.; Netz, R. Ionic Force Fields for Divalent Cations in Salt Solutions Based on Their Single-Ion and Ion-Pair Properties. *J. Chem. Phys.* **2013**, *138* (2), 24505.